

Supporting Information for “Spectral decomposition of internal gravity wave sea surface height in global models”

Anna C. Savage,¹ Brian K. Arbic,² Matthew H. Alford,³ Joseph K. Ansong,²
J. Thomas Farrar,⁴ Dimitris Menemenlis,⁵ Amanda K. O’Rourke,² James G.
Richman,⁶ Jay F. Shriver,⁷ Gunnar Voet,³ Alan J. Wallcraft,⁷ Luis Zamudio⁶

¹Applied Physics Program, University of
Michigan, Ann Arbor, Michigan, USA

²Department of Earth and Environmental
Sciences, University of Michigan, Ann
Arbor, Michigan, USA

³Scripps Institution of Oceanography,
University of California, San Diego, La Jolla
California, USA

⁴Physical Oceanography Department,
Woods Hole Oceanographic Institution,
Woods Hole, MA, USA

⁵Earth Sciences Division, Jet Propulsion
Laboratory, California Institute of
Technology, Pasadena, CA, USA

Contents of this file

1. Figures S1 to S8

Introduction

This file consists of eight figures that accompany the paper “Spectral decomposition of internal gravity wave sea surface height (SSH) in global models”. These figures were not included in the manuscript for the sake of brevity of the journal article. In the article, frequency-horizontal wavenumber sea surface height variance spectral densities are computed from two simulations of the HYbrid Coordinate Ocean Model (HYCOM) and three simulations of the Massachusetts Institute of Technology general circulation model (MITgcm) in seven regions of the world ocean. For the sake of brevity, the frequency-horizontal wavenumber spectral densities computed in all regions of only one simulation are shown in the main article file. Figures S1-S8 show the SSH frequency-horizontal wavenumber spectral densities in all seven regions in the remaining four simulations. This article also investigates the frequency content to wavenumber by integrating the frequency-horizontal wavenumber spectral densities over three frequency bands of interest:

⁶Center for Oceanic-Atmospheric

Prediction Studies, Florida State University,

Tallahassee, Florida, USA

⁷Oceanography Division, Naval Research

Laboratory, Stennis Space Center,

Mississippi, USA

the subtidal band [$\omega < 0.86$ cpd], the tidal band [$0.87 < \omega < 2.05$ cpd], and the supertidal band [$\omega > 2.06$ cpd]. Again, the article shows the frequency band integrated wavenumber spectral densities in all regions in just one simulation. Figures S5-S8 show the horizontal wavenumber spectral densities in all regions in the remaining four simulations.

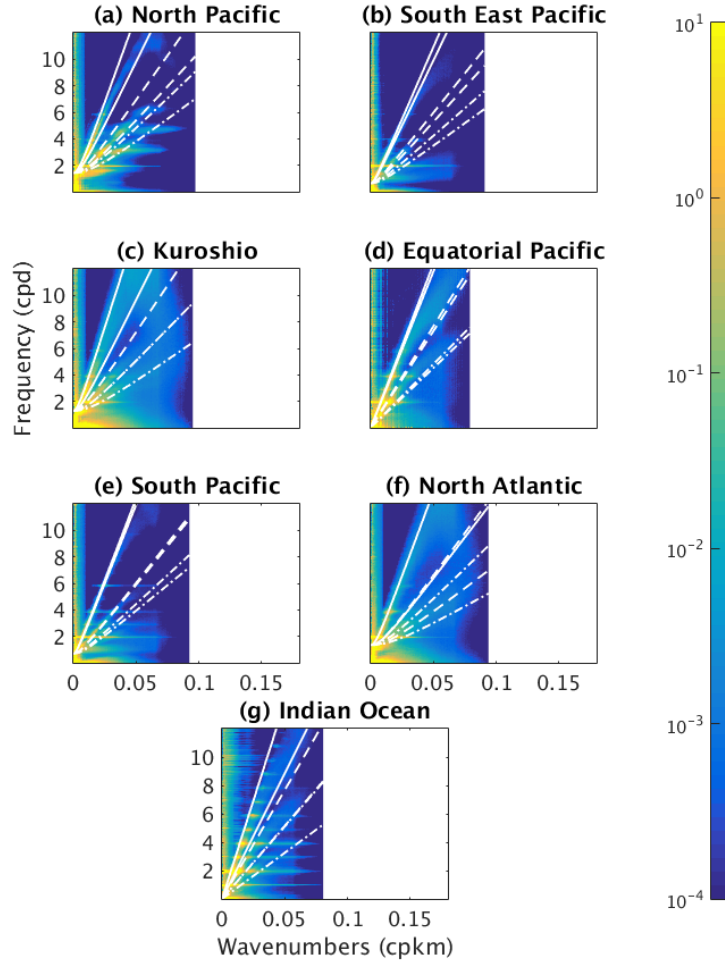


Figure 1. Frequency-horizontal wavenumber spectral density of SSH variance [$\text{cm}^2/(\text{cpd cpkm})$] computed over seven regions from HYCOM12. Wavenumber axes are set to the maximum wavenumber for each region computed in HYCOM25. White curves show theoretical IGW linear dispersion relations for first (solid), second (dashed), and third (dashed-dotted) vertical modes. Bounding curves for each vertical mode are computed from the maximal and minimal eigenspeeds along the northern and southern boundaries, as in *Müller et al.* [2015].

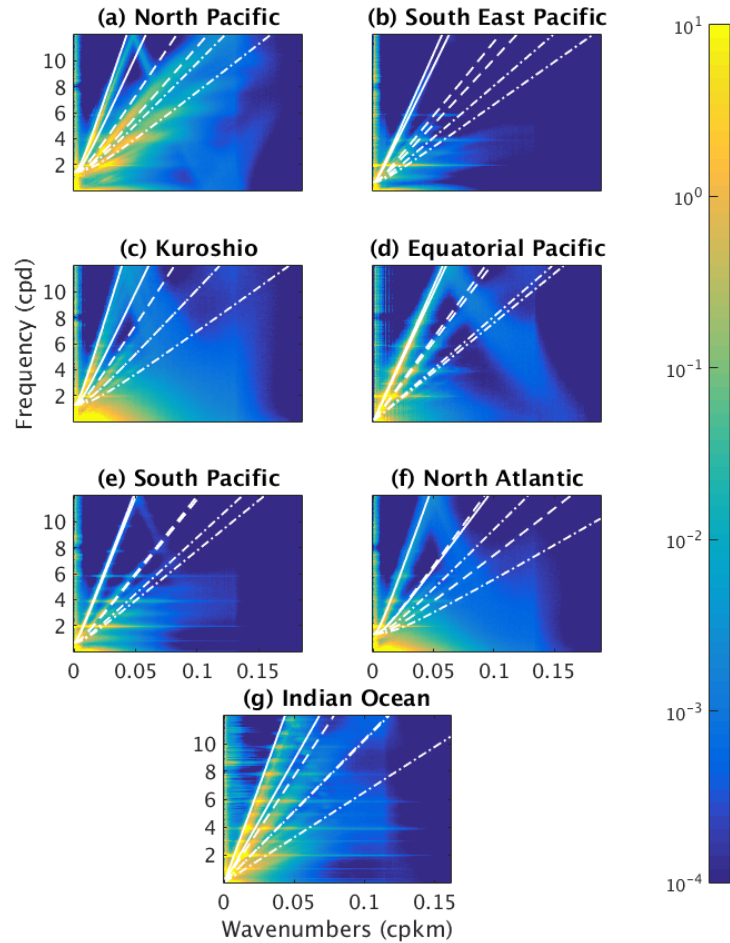


Figure 2. Frequency-horizantal wavenumber spectral density of SSH variance [$\text{cm}^2/(\text{cpd cpkm})$] computed over seven regions from HYCOM25. Wavenumber axes are set to the maximum wavenumber for each region computed in HYCOM25. White curves show theoretical IGW linear dispersion relations for first (solid), second (dashed), and third (dashed-dotted) vertical modes. Bounding curves for each vertical mode are computed from the maximal and minimal eigenspeeds along the northern and southern boundaries, as in *Müller et al.* [2015].

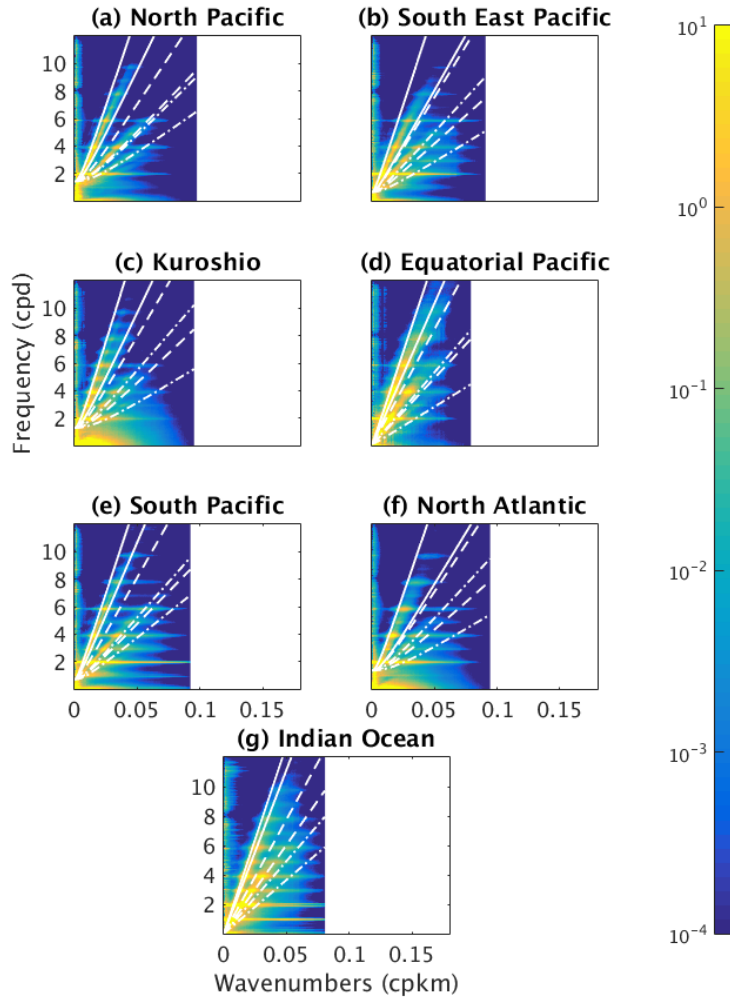


Figure 3. Frequency-horizontal wavenumber spectral density of SSH variance [$\text{cm}^2/(\text{cpd cpkm})$] computed over seven regions from MITgcm12. Wavenumber axes are set to the maximum wavenumber for each region computed in HYCOM25. White curves show theoretical IGW linear dispersion relations for first (solid), second (dashed), and third (dashed-dotted) vertical modes. Bounding curves for each vertical mode are computed from the maximal and minimal eigenspeeds along the northern and southern boundaries, as in *Müller et al.* [2015].

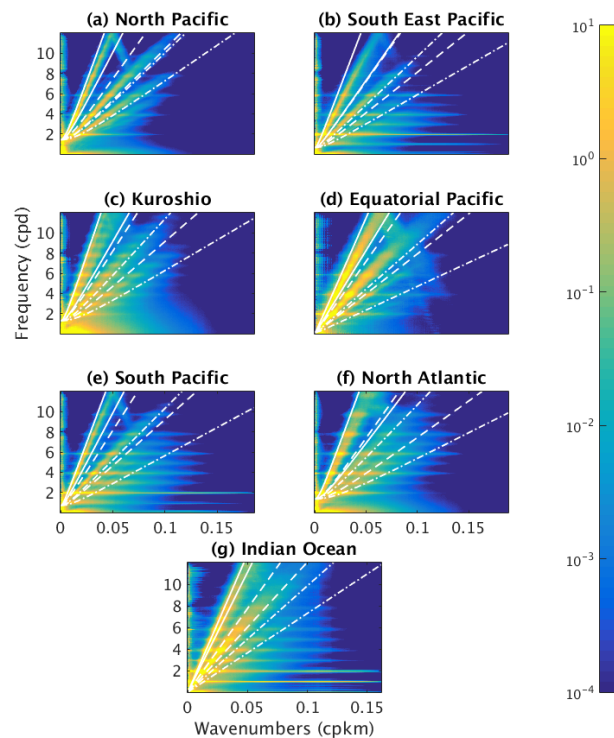


Figure 4. Frequency-horizontal wavenumber spectral density of SSH variance [$\text{cm}^2/(\text{cpd cpkm})$] computed over seven regions from MITgcm24. Wavenumber axes are set to the maximum wavenumber for each region computed in HYCOM25. White curves show theoretical IGW linear dispersion relations for first (solid), second (dashed), and third (dashed-dotted) vertical modes. Bounding curves for each vertical mode are computed from the maximal and minimal eigenspeeds along the northern and southern boundaries, as in *Müller et al.* [2015].

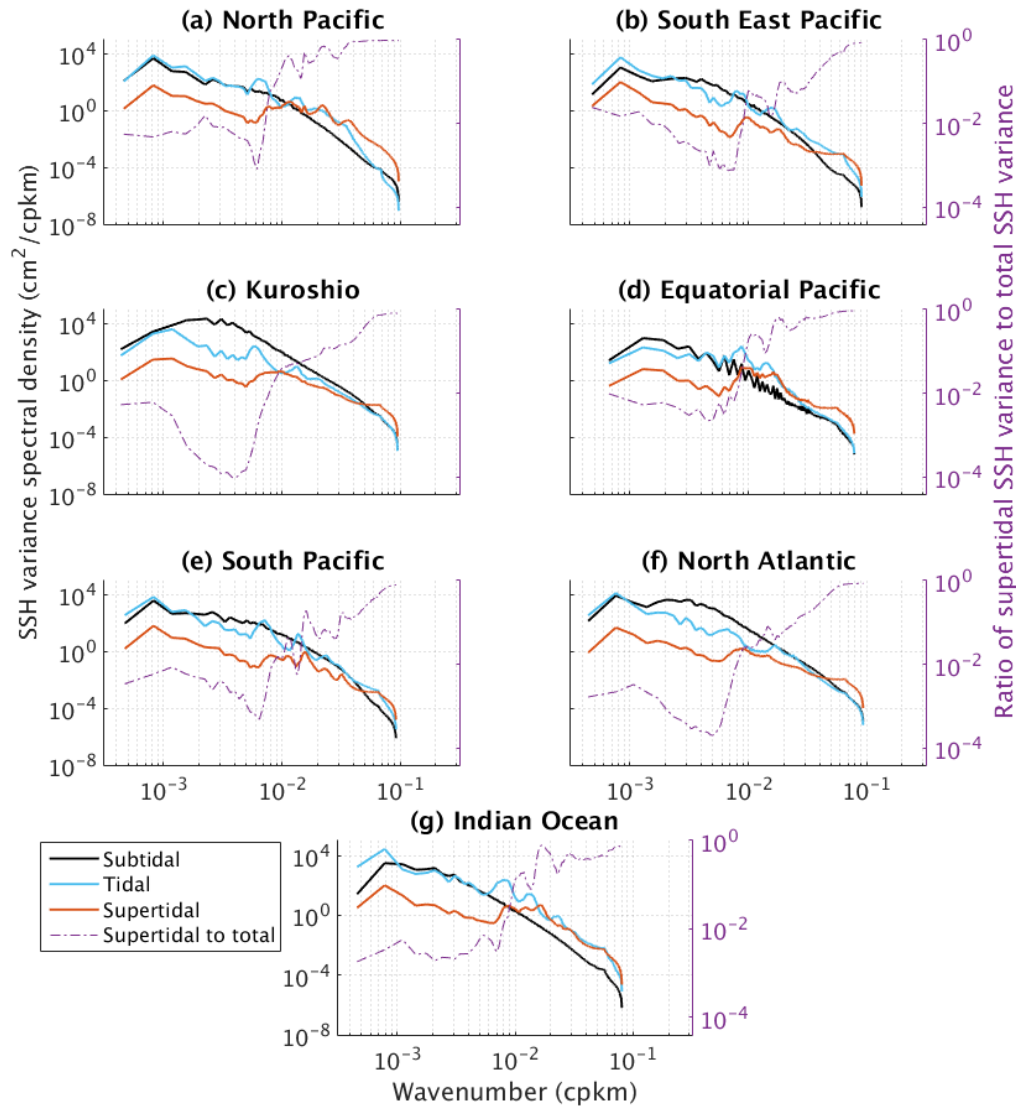


Figure 5. Horizontal wavenumber SSH variance spectral density in all regions in HYCOM12 integrated over subtidal, tidal, and supertidal frequency bands (see text for definition of bands). The 95% confidence intervals span 76% to 137% of shown value for the subtidal band, 85% to 119% for the tidal band, and 94% to 107% for the supertidal band. Right-hand axis shows ratio of supertidal to total SSH variance as a function of isotropic wavenumber.

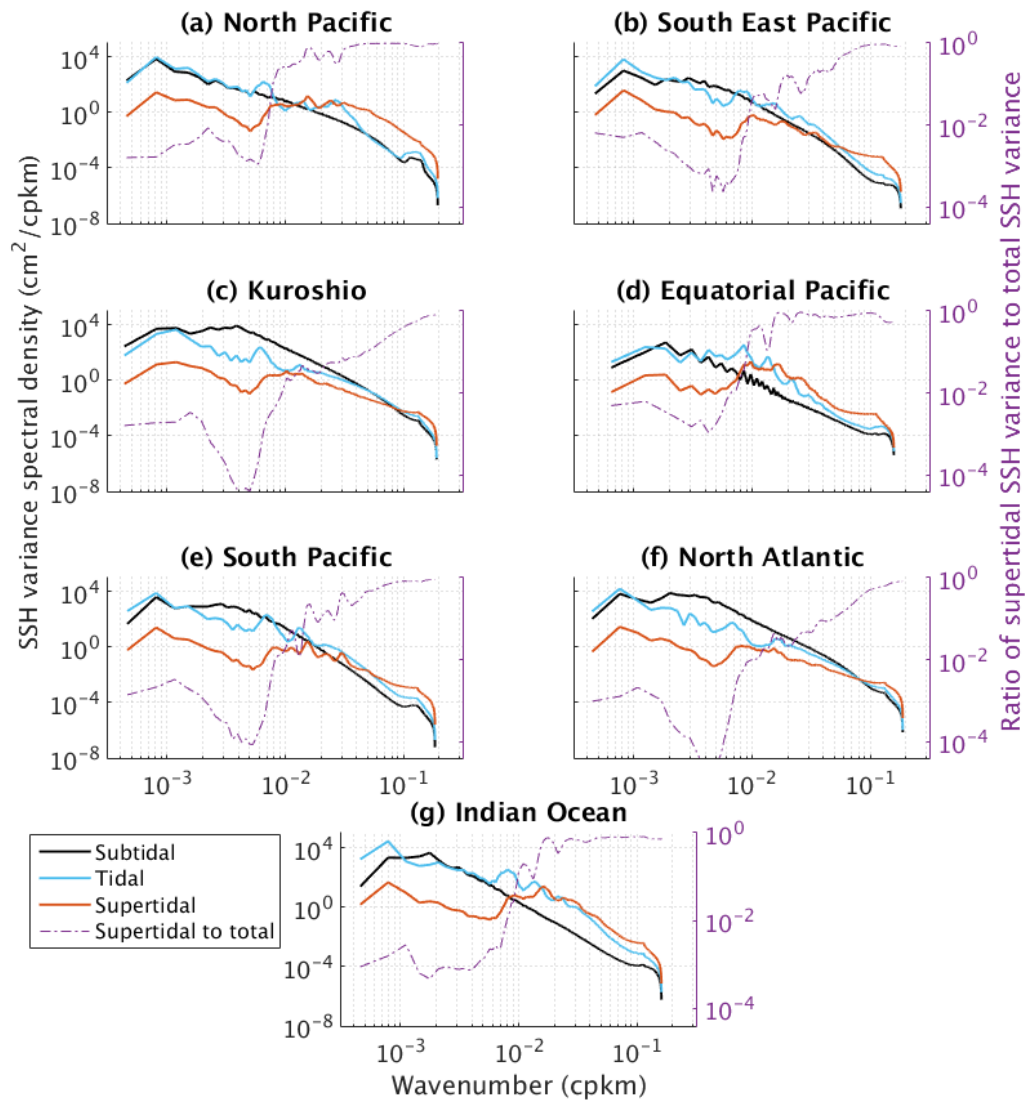


Figure 6. Horizontal wavenumber SSH variance spectral density in all regions in HYCOM25 integrated over subtidal, tidal, and supertidal frequency bands (see text for definition of bands). The 95% confidence intervals span 76% to 137% of shown value for the subtidal band, 85% to 119% for the tidal band, and 94% to 107% for the supertidal band. Right-hand axis shows ratio of supertidal to total SSH variance as a function of isotropic wavenumber.

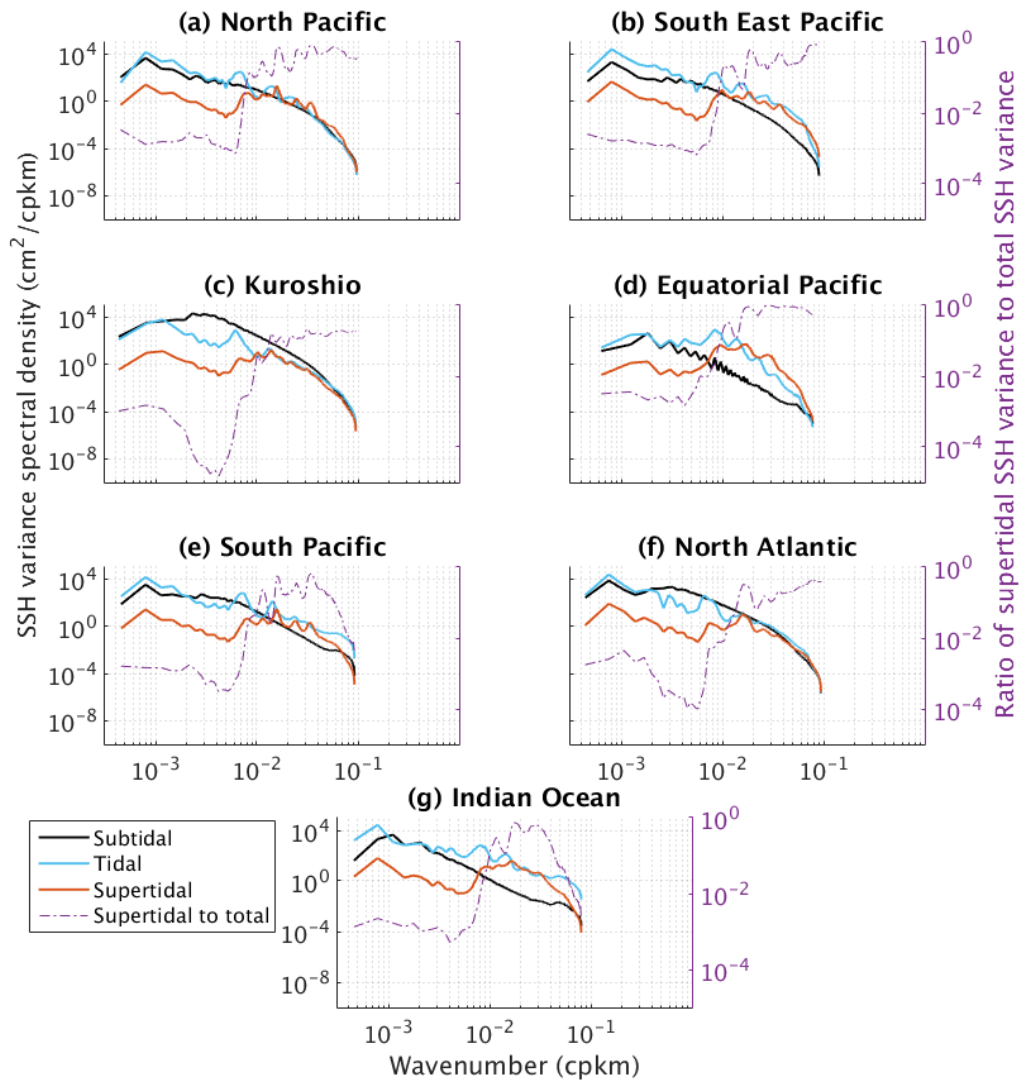


Figure 7. Horizontal wavenumber SSH variance spectral density in all regions in MITgcm12 integrated over subtidal, tidal, and supertidal frequency bands (see text for definition of bands). The 95% confidence intervals span 76% to 137% of shown value for the subtidal band, 85% to 119% for the tidal band, and 94% to 107% for the supertidal band. Right-hand axis shows ratio of supertidal to total SSH variance as a function of isotropic wavenumber.

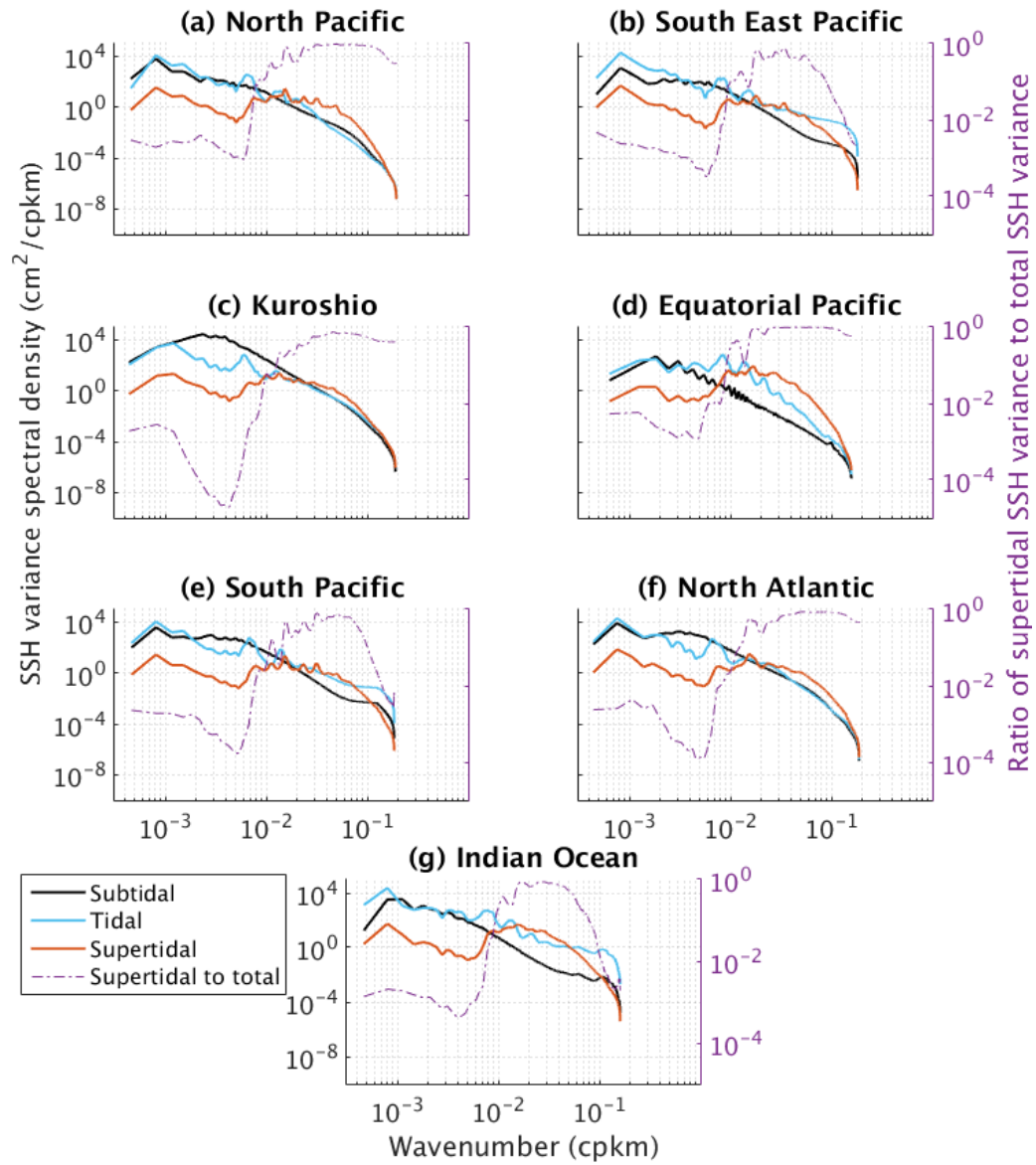


Figure 8. Horizontal wavenumber SSH variance spectral density in all regions in MITgcm24 integrated over subtidal, tidal, and supertidal frequency bands (see text for definition of bands). The 95% confidence intervals span 76% to 137% of shown value for the subtidal band, 85% to 119% for the tidal band, and 94% to 107% for the supertidal band. Right-hand axis shows ratio of supertidal to total SSH variance as a function of isotropic wavenumber.